ARTICLE

Invited Contribution from Award Winners of the 21st National Electrochemical Congress in 2023

Sorbitol-Electrolyte-Additive Based Reversible Zinc Electrochemistry

Qiong Sun [a], Hai-Hui Du [a], Tian-Jiang Sun [a], Dian-Tao Li [a], Min Cheng [a], Jing Liang [a,*], Hai-Xia Li [a,b,*], Zhan-Liang Tao [a]

[a] Key Laboratory of Advanced Energy Materials Chemistry (Ministry of Education), Collaborative Innovation Center of Chemical Science and Engineering (Tianjin), Renewable Energy Conversion and Storage Center (RECAST), College of Chemistry, Nankai University, Tianjin, 300071, China
[b] Key Laboratory of Advanced Electrode Materials for Novel Solar Cells for Petroleum and Chemical Industry of China, School of Chemistry and Life Sciences, Suzhou University of Science and Technology, Suzhou 215009, Jiangsu, China

Abstract

The unstable zinc (Zn)/electrolyte interfaces formed by undesired dendrites and parasitic side reactions greatly hinder the development of aqueous zinc ion batteries. Herein, the hydroxy-rich sorbitol was used as an additive to reshape the solvation structure and modulate the interface chemistry. The strong interactions among sorbitol and both water molecules and Zn electrode can reduce the free water activity, optimize the solvation shell of water and Zn^{2+} ions, and regulate the formation of local water (H_2O)-poor environment on the surface of Zn electrode, which effectively inhibit the decomposition of water molecules, and thus, achieve the thermodynamically stable and highly reversible Zn electrochemistry. As a result, the assembled Zn/Zn symmetric cells with the sorbitol additive realized an excellent cycling life of 2000 h at 1 $mA \cdot cm^{-2}$ and 1 $mAh \cdot cm^{-2}$, and over 250 h at 5 $mA \cdot cm^{-2}$ and 5 $mAh \cdot cm^{-2}$. Moreover, the Zn/Cu asymmetric cells with the sorbitol additive achieved a high Coulombic efficiency of 99.6%, obtaining a better performance than that with a pure 2 $mol \cdot L^{-1}$ $ZnSO_4$ electrolyte. And the constructed Zn/poly1, 5-naphthalenediamine (PNDA) batteries could be stably discharged for 2300 cycles at 1 $A \cdot g^{-1}$ with an excellent capacity retention rate. This result indicates that the addition of 1 $mol \cdot L^{-1}$ non-toxic sorbitol into a conventional $ZnSO_4$ electrolyte can successfully protect the Zn anode interface by improving the electrochemical properties of Zn reversible deposition/decomposition, which greatly promotes its cycle performance, providing a new approach in future development of high performance aqueous Zn ion batteries.

Keywords: Aqueous zinc ion batteries; Dendrite; Sorbitol additive; Solvation regulation; Interface modulation

1. Introduction

Electrochemical energy storage technology has irreplaceable social value in the low-carbon transition process of replacing traditional fossil fuels with new energy [1]. Lithium ion batteries have such advantages as high specific energy density and high energy efficiency [2], however, the potential risks to safety, limited resources, high expenses, and other problems are still being given more consideration [3,4]. Aqueous zinc ion batteries (AZIBs) have attracted great attention due to their excellent safety, cost-effectiveness, and environmental friendliness, and are considered one of the promising candidates for large-scale energy storage. Despite these advantages, AZIBs still suffer from various unfavorable bottlenecks such as dendrite growth, corrosion, hydrogen evolution

Received 29 November 2023; Received in revised form 18 February 2024; Accepted 23 February 2024
Available online 28 February 2024

*Corresponding author, Haixia Li, E-mail address: lihaixia@nankai.edu.cn.
*Corresponding author, Jing Liang, E-mail address: liangjing@nankai.edu.cn.

https://doi.org/10.61558/2993-074X.3447

reaction (HER) and by-products, which hamper the large-scale implementation of AZIBs. Due to the thermodynamic limitation, the equilibrium potential of H_2O/H_2 is higher than that of Zn^{2+}/Zn in the entire pH range, indicating the spontaneous hydrogen gas evolution and corrosion on the anode surface [5,6]. Subsequently, in the $ZnSO_4$ electrolyte, the elevation of the pH value of electrolytes and the residual OH^- ions will aggravate the formation of by-products ($Zn_4SO_4(OH)_6 \cdot xH_2O$), with randomly accumulating on the Zn surface, which impedes ion/electron diffusion and negatively affects the Zn reversibility, and this strongly bound zincate complex will further promote the formation of zinc dendrites [7]. It is widely acknowledged that the aqueous electrolyte contains two types of water molecules: free water molecules and solvated water molecules [8]. Furthermore, Zn^{2+} ions tend to form a close ion pair with free water molecules during the electrodeposition process [9], which produces a great deal of active water molecules in the anode/electrolyte interface, thus leading to various side reactions [10]. Therefore, inhibition of dendritic and parasitic reactions is necessary to improve the reversibility of zinc anodes by regulating the solvation shell structures around zinc ions and designing suitable interface layers [11].

The electrolyte is one of the most important components in Zn-based energy storage devices due to the bridge function of connecting the cathode and anode while providing a pathway for Zn ions migration [12]. Recent studies on electrolytes optimization, including the incorporation of co-solvents to form aqueous eutectics [13,14], application of salt-concentrated electrolytes [15], construction of artificial protective layers [16,17], have been explored, despite this, their expensive price tag, large viscosity, and other characteristics impede their further development. Developing cost-effective electrolyte formulations with decreased water activity but excellent stability and ion transport could potentially enhance the effectiveness and durability of zinc anode in aqueous AZIBs. The introduction of appropriate molecular additives with strong complexation with Zn^{2+} in electrolyte systems should be an effective and low-cost solution that can destroy the original Zn^{2+} solvation structure [18]. Furthermore, comprehending the intricate chemical interactions between the additive and the bulk electrolyte or zinc anode surface, as well as its potential to improve solvation structure, inhibit free water activity, and regulate interfacial behavior to mitigate interfacial side reactions [19], is an exceedingly promising field.

We hereby propose an eco-friendly sorbitol ($C_6H_{14}O_6$, SOR) electrolyte addictive system. Zinc sulfate ($Zn(SO_4)$, 2 $mol \cdot L^{-1}$) was employed as the primary electrolyte (ZSO), with the sorbitol content (x) ranging from 0.5 $mol \cdot L^{-1}$ to 13 $mol \cdot L^{-1}$, a series of the ZSO-SOR-x $mol \cdot L^{-1}$ electrolytes were prepared to simultaneously enhance Zn stripping/plating reversibility. The molecular dynamics simulations show that sorbitol had a good performance in regulating the solvation structure, and achieved better performance in inhibiting the growth of Zn dendrites and various side reactions. Simultaneously, SOR has a strong attraction to both H_2O molecules and Zn electrodes, with a high concentration of hydroxyl groups, creating an intermolecular hydrogen bond with water molecules, thus decreasing the activity of the water molecules that are bound, and changing the environment for Zn deposition. It is also found that the wettability and anti-corrosion capability of Zn anode were improved with the uniformed distribution of Zn^{2+} ions, as well as the two-dimensional (2D) diffusion is limited and the dendrite growth is inhibited. Accordingly, the Zn/Zn symmetric cell exhibited exceptional cyclability over 2000 h under 1 $mA \cdot cm^{-2}$ and 1 $mAh \cdot cm^{-2}$, and the full battery achieved an extended cycle life of 2300 cycles when coupled with poly1,5-naphthalenediamine (PNDA) at 1 $A \cdot g^{-1}$. More importantly, this additive electrolyte strategy outperforms the others the projected cost, providing a viable solution for application-oriented AZIBs.

2. Experimental section

$ZnSO_4 \cdot 7H_2O$ (Sigma Aldrich) was dissolved in deionized water to prepare 2 $mol \cdot L^{-1}$ $ZnSO_4$ electrolyte (ZSO) as the baseline electrolyte. Stoichiometric amounts of sorbitol (0.45 g, 0.91 g, 1.82 g, 2.73 g, 3.64 g, 4.55 g, 6.37 g, 9.1 g, 11.83 g) were dissolved into 5 mL 2 $mol \cdot L^{-1}$ $ZnSO_4$ electrolyte to formulate ZSO-SOR-0.5, 1, 2, 3, 4, 5, 7, 10, 13 M electrolytes, respectively.

To prepare poly1, 5-naphthalenediamine (PNDA) cathode, 6.8 mmol 1, 5-naphthalenediamine was dissolved in 100 mL 0.1 $mol \cdot L^{-1}$ HCl, and violently stirred in an ice water bath, then 10 mmol $K_2S_2O_8$ was added to the mixed solution in a small amount for several times, and the reaction was carried out in an ice water bath for 24 h. The filtered products were washed with deionized water, DMF and ethanol successively. The product was then dried under a vacuum at 60 °C for 24 h.

The PNDA electrodes were prepared by mixing the as-prepared PNDA powers, Ketjen black (KB), and polytetrafluoroethylene (PTFE) with the weight ratio of 7:2:1. The mixture was compressed into slices and cut into wafers with a diameter of 8 mm, then the wafers were pressed onto stainless

steels mesh (Φ 12 mm) and dried at 80 °C for 12 h under a vacuum. The coin cells were assembled in an air, using zinc metal (0.05 mm, Φ 12 mm) as the anode, ZSO-SOR-1 M as the electrolyte, and glass fiber (Φ 16 mm) as the separator. The electrochemical performances of these cells were evaluated in the voltage range of 0.2−1.8 V versus Zn^{2+}/Zn with a LAND multichannel battery test system.

Chronoamperometric (CA) curves were obtained from an electrochemical workstation (CHI660B) at a fixed overpotential of −150 mV in Zn symmetric cells. Electrochemical impedance spectroscopic (EIS) data were measured over the frequency range of 10 kHz to 1 Hz. The hydrogen evolution reaction behaviors were recorded using linear sweep voltammetry (LSV) at a sweep rate of 1 $mV \cdot s^{-1}$, Cyclic voltammetry (CV) was used to test Zn/PNDA full cells at a scan rate of 10 $mV \cdot s^{-1}$.

Proton magnetic resonances (^{1}H NMR) were conducted on a Bruker Avance III 400 MHz. Fourier Transform Infrared Spectroscopic (FTIR) curve was recorded with a Bruker 46 TENSOR II. X-ray diffraction (XRD) tests were performed on a SmartLab 9 kW with Cu $K\alpha$ radiation and the diffraction data were collected at a step mode over the angular range of 5°−80°. The microstructure and morphology were observed by field-emission scanning electron microscope (FE-SEM, JSM-7900F) equipped with energy dispersive spectroscope (EDS) for elemental analysis.

3. Theory calculations

The binding energy (E_b) between two components is performed by the Vienna Ab-initio Simulation Package (VASP), and the exchange-correlation energy is approximately described by the Perdew-Burke-Ernzerhof (PBE) functional based on the generalized gradient approximation (GGA). In all calculations, a cut-off energy with the value of 550 eV is used for the plane wave basis, and the convergence criteria for the ionic relaxation and the electronic self-consistent calculation are set to −0.05 eV/Å and 10^{-5} eV, respectively. The anions are modeled by adding electrons to the system. The Zn (0001) surface is modeled by a three-layer 8 × 4 surface supercell (32 Zn atoms per layer), and a vacuum region of 20 Å is set to avoid undesirable interactions arising from period boundary conditions. The adsorption energies (E_{ads}) are calculated as $E_{ads} = E_{ad/sub} - E_{ad} - E_{sub}$, where $E_{ad/sub}$, E_{ad} and E_{sub} are the optimized adsorbate/substrate system, the adsorbate in the structure and the clean substrate, respectively.

Density functional theory (DFT) calculations, and the HOMO (Highest occupied molecular orbital) and LUMO (Lowest unoccupied molecular orbital) orbitals are performed by using the Gaussian 16 program 3, which the Gaussian format checkpoint file is used as the input file. Geometry optimization and frequency analyses are performed using the SMD solvation model of water. C, H, O, use B3LYP functional and 6-31+G (d, p) basis set.

The partial charge and parametric information (bond parameters, angle parameters and the dihedral angles and so on) of sorbitol molecule is calculated using Automated Topology Builder (ATB), and Repository and the GROMOS 54A7 force field are applied [20]. The 36 Zn^{2+} ions, 36 SO_4^{2-} ions, 18 sorbitol molecules and 1000 water molecules are randomly inserted into a cube box with a side length of 8.00 nm. The molecular dynamics (MD) simulation for the interaction among the Zn^{2+} ions, SO_4^{2-} ions, sorbitol and water molecules are performed in the GROMACS 2019 software package [21].

After 10 ns of MD simulations, we extracted the data to analyze the radial distribution function (RDF) and coordination number (CN) between Zn^{2+} ions and SO_4^{2-} ions, and O atom in water and sorbitol. The form of hydrogen bonding in this system is explored. The numbers of hydrogen bonds among sorbitol molecules and water molecules, water molecules and water molecules and whole system are calculated.

4. Results and discussion

In order to investigate the effect of SOR on the electrochemical performance of hybrid electrolytes, a series of theoretical calculations and spectroscopic analyses were combined for better understanding. Molecular dynamics (MD) simulations of the solvated structure of Zn^{2+} in 2 $mol \cdot L^{-1}$ $ZnSO_4$ and ZSO-SOR-1 M are first performed, where Zn^{2+} is surrounded by a solvated sheath of H_2O and SO_4^{2-} in the $ZnSO_4$ system (Fig. 1a), the original solvation shell is composed of H_2O and SO_4^{2-} in a ratio of 4.7:1.3. However, when sorbitol molecules enter the solvation sheath of Zn^{2+} in the $ZnSO_4$ system (Fig. 1a right), the average coordination numbers of Zn^{2+}-H_2O, Zn^{2+}-SO_4^{2-} and Zn^{2+}-SOR are ≈4.35, ≈1.24 and ≈0.41, respectively. This indicates that SOR enters the first solvation shell of Zn^{2+} by displacing H_2O molecules. Then the diffusion rates of Zn^{2+} in these electrolytes are calculated, which can be qualitatively evaluated by the mean-squared displacement (MSD) as a function of time (Fig. 1b), indicating that the Zn^{2+} diffusion rate is inversely proportional to SOR concentration. The addition of sorbitol can effectively modify the solvation structure, as demonstrated by this section of the calculation. As the concentration rises, the proportion of

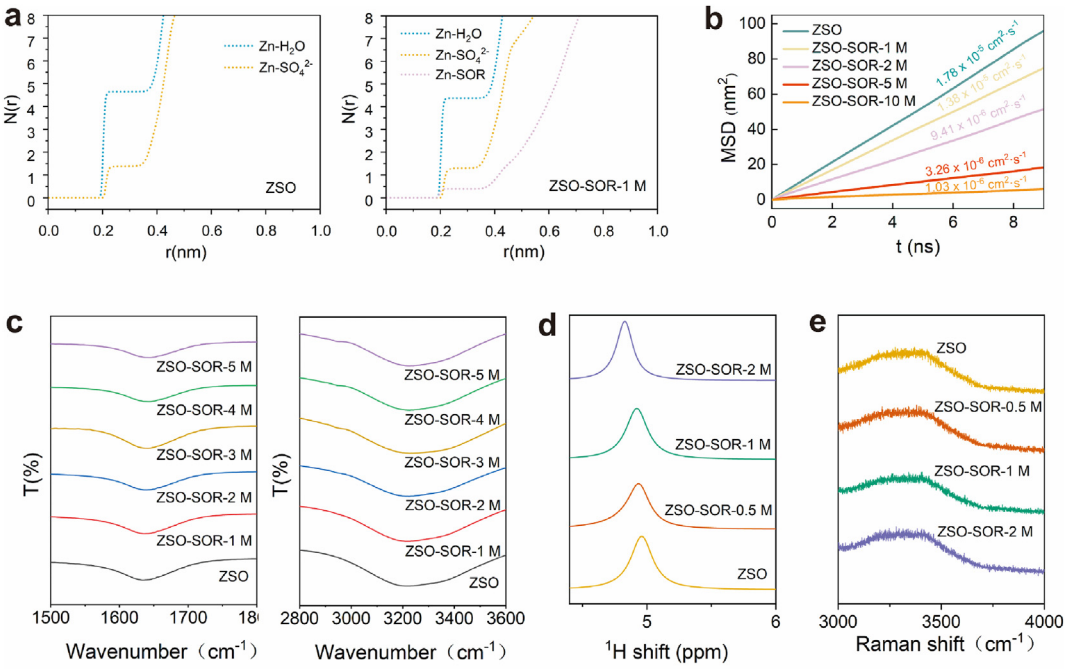

Fig. 1. (a) The average coordination numbers of Zn-H_2O, Zn-SO_4^{2-} and Zn-SOR collected from MD simulations in ZSO and ZSO-SOR-1 M electrolytes. Electrolyte addition at different concentrations of SOR: (b) MSD plots, (c) FTIR spectra, (d) ^1H NMR spectra, (e) Raman spectra.

combined water molecules decreases continuously (Figure S1), however, the diffusion rate of Zn^{2+} will gradually decrease, thus affecting the overall performance of the battery. Fourier Transform Infrared spectroscopy (FTIR), Raman spectroscopy, and Nuclear Magnetic Resonance (NMR) were employed to explore the influence of ZSO-SOR-*x* M electrolyte systems. The FTIR spectrum indicates an unignorable blue shift in the OH stretching vibration at 3000−3500 cm^{-1} and a slight blue shift in the bending vibration of H_2O at 1600−1700 cm^{-1} as the SOR content increases (Fig. 1c), implying hydrogen bonds (HB) between SOR and H_2O. Also, the OH stretching band (3200−3400 cm^{-1}) of H_2O in the Raman spectra shifts to higher wavenumbers with the increasing SOR content (Fig. 1e), verifying the HB of SOR-H_2O. Meanwhile, in the ^1H NMR spectra (Fig. 1d), the chemical shift of ^1H from H_2O in the hybrid electrolytes continually decreases, and moves to higher field, as the SOR content increases, indicating higher electron cloud density of ^1H from H_2O [22], which may be attributed to the hydrogen bond interaction between the O atoms in SOR and the H atoms in H_2O. The collective spectral findings suggest that sorbitol has the ability to establish a hydrogen bond network with water molecules, resulting in the disruption of the hydrogen bond network among water molecules, inhibiting the activity of water molecules [23], augmenting the energy requirement for electrochemical water decomposition [24], thus, suppressing side reactions on the zinc anode, and enhancing the efficiency of AZIBs.

Coulombic efficiency (CE) is a key parameter for evaluating Zn reversibility. In the asymmetric Zn/Ti cell, the CE dropped to zero after 19 cycles in the ZSO electrolyte. Nevertheless, it demonstrates higher CE (average 97% after the stability test) and longer cycle life (250 cycles) in ZSO-SOR-1 M electrolyte (Figure S2). When the concentration of sorbitol increased to 2 mol·L^{-1}, the CE of Zn/Ti asymmetric cell began to decline. This may be caused by the slower Zn^{2+} transport with increasing concentration, which also corresponds to the calculation results of MSD in the previous article. Meanwhile, we measured their ion conductivity (Fig. 2b) through electrochemical impedance spectroscopy (EIS) (Figure S3), and found that the ion conductivity of the electrolyte gradually decreased as the SOR content increased, when the SOR concentration was 1 mol·L^{-1}, the ionic conductivity of the electrolyte maintained 32.1 mS·cm^{-1}. However, the conductivity continued to decrease as the concentration increased, when the concentration of the sorbitol rose to 2 mol·L^{-1}, its ionic conductivity decreased to 19.9 mS·cm^{-1}. The low ionic conductivity leads to the low internal mass transfer rate of the electrolyte, which aggravates the concentration polarization of the electrode surface. When the concentration is too high, the wettability between the electrolyte and the zinc anode will also become worse, and the uneven electric field will affect the

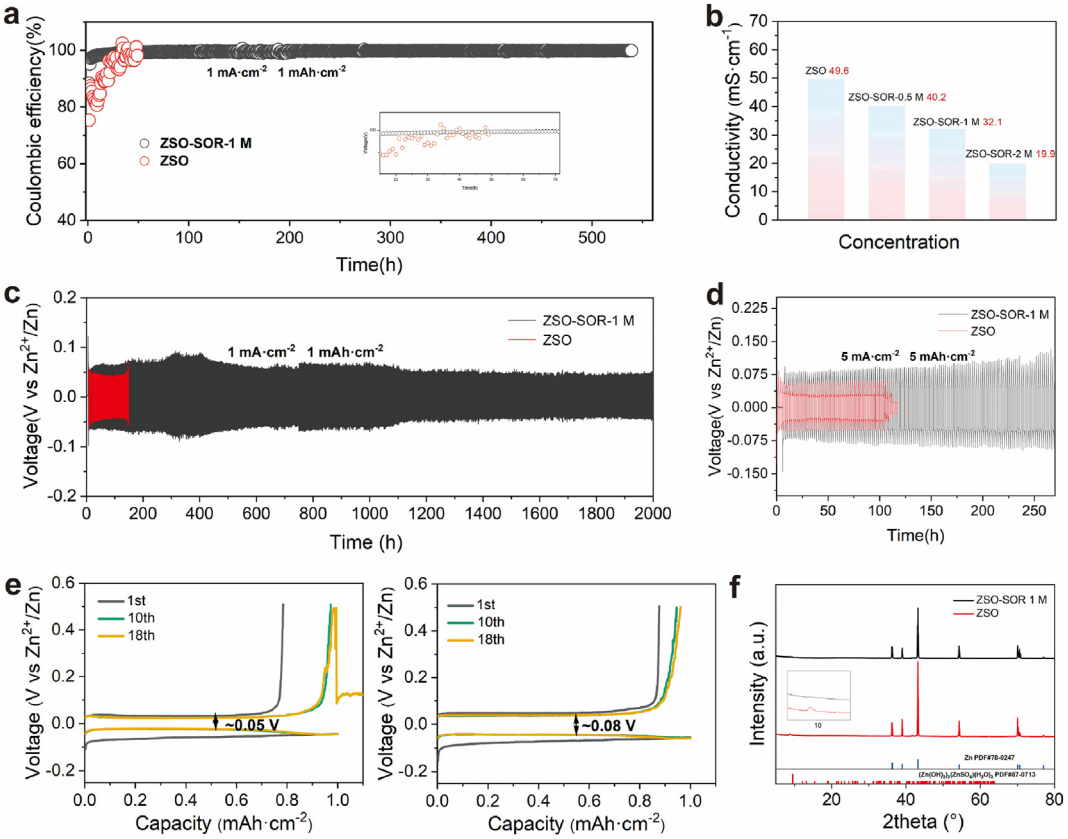

Fig. 2. (a) CEs of the Zn/Cu asymmetric cells tested with a current density of 1 mA·cm^{-2} and a cut off charging voltage of 0.5 V. (b) Schematic representation of the conductivity at different SOR concentrations. Long-term galvanostatic Zn stripping/plating in the Zn/Zn symmetric cells under (c) 1 mA·cm^{-2}, 1 mAh·cm^{-2} and (d) 5 mA·cm^{-2}, 5 mAh·cm^{-2}. (e) Voltage profiles and deposition-stripping curves of ZSO (left) and ZSO-SOR-1 M (right) electrolyte Zn/Ti cells. (f) XRD patterns of the fabricated Zn layer after 100 cycles in the ZSO and ZSO-SOR-1 M electrolytes at 1 mAh·cm^{-2} (The inset plot is a local magnification of the XRD of the two curves at 6°−14°).

uniform deposition of the zinc anode surface. To conclude, ZSO-SOR-1 M was chosen as the focus of further investigation. In the asymmetric Zn/Cu cell, compared with the ZSO electrolyte, the ZSO-SOR-1 M modified electrolyte achieved a high average CE of 99.6% after 500 cycles under the test condition of 1 mA·cm^{-2} and 1 mAh·cm^{-2} (Fig. 2a). This indicates that the presence of SOR effectively inhibits the by-products generated during the cycle, and improves the cycle efficiency and lifetime. In addition, the deposition/stripping curve of the asymmetric Zn/Ti cell was measured (Fig. 2e), and it can be seen that the deposition/stripping curves of the ZSO electrolyte were no longer stable after 18 cycles. Moreover, the overpotential of ZSO-SOR-1 M was slightly larger by 0.03 V than that of the ZSO electrolyte, which indicates that certain adsorption behavior occurs at the anode interface of zinc in the mixed electrolyte.

The cycling stability of the Zn electrode was investigated in symmetric cells. Compared to the Zn/Zn symmetric cell with ZSO electrolyte operating for 198 h, the ZSO-SOR-1 M electrolyte cell enabled an ultralong cycle life of 2000 h at 1 mAh·cm^{-2} with a fixed plating/stripping time of 1 h (Fig. 2c). When further increasing the current density to 5 mA·cm^{-2}, the ZSO and ZSO-SOR-1 M electrolyte cases exhibit cycle life of 100 h and 270 h (Fig. 2d), respectively. Combined with the depositing/stripping curve of the asymmetric Zn/Ti cell (Fig. 2e), this may be related to SOR adsorption on the plating interface (detailed in the following section), indicating that the electrolyte added of SOR has a better ability to regulate the changes of the interface electric field [16]. In addition to this concentration, we also tested the electrochemical performance of other electrolytes added at higher concentrations, and it can be seen that compared with the base ZSO electrolyte, the performance of the added group was improved to varying degrees (Figure S4).

X-ray Powder diffractometer (XRD) testing was conducted on zinc sheets after 100 cycles in the electrolyte before and after modification under 1 mAh·cm^{-2} (Fig. 2f). In the electrolyte of ZSO, a slight summit at 8.9° emerged, indicating the presence of basic zinc sulfate, which can be attributed to the increase of pH in the local region due to hydrogen evolution, and the peak of by-product was not observed on the zinc sheet after

circulating in the ZSO-SOR-1 M electrolyte, which also verified that the hydrogen bond formed between sorbitol and water molecules inhibited the side reaction, thus inhibiting the electrochemical corrosion of the zinc anode.

The electrochemical deposition process is closely related to interfacial stability, so the studying in interfacial adsorption behavior is necessary. The cyclic voltammetric (CV) curve of zinc-symmetric cell in a pure SOR solution appears no redox peak (Figure S5), which indicates that the SOR solution performs non-Faraday adsorption at the interface [25]. It can be seen that the contact angle between ZSO-SOR-1 M electrolyte and Zn anode interface is the smallest, which shows good wettability (Fig. 3c). The favorable adsorption behavior of SOR is attributed to its abundant zincophilic hydroxyl groups, when sorbitol is adsorbed on the surface of Zn anode, the hydroxyl groups can attract Zn ions, and disperse the flux of Zn ions flux and inhibit the deposition of Zn ions at the top [26], thus promoting the uniform deposition of Zn ions. Density functional theory (DFT) is used to probe the structure of Zn/electrolyte interface [27] (Fig. 3a), and the corresponding adsorption configurations are shown in Figure S6. Compared with water molecules, the higher adsorption energies of SOR and Zn mean that the interfacial adsorption of SOR is better, indicating that SOR can play a role in the isolation of water molecules through the molecular adsorption at the interface. At the same time, further calculations reveal that the hydroxyl terminal group of SOR molecule has a higher priority in binding with the Zn interface. The interaction between SOR and Zn interface is thermodynamically favorable, which is also supported by the energy of the highest occupied orbital (HOMO). The HOMO value follows SOR > H_2O (Fig. 3b), which suggests that the interaction between the hydroxyl group of SOR adsorbed on the Zn electrode with the Zn anode is more preferential [16].

Chronomperometric (CA) measurements of the ZSO and ZSO-SOR-*x* M electrolytes were carried out to investigate the electrodeposition process of Zn electrodes [28]. When the bias voltage was −150 mV, the current response of the base

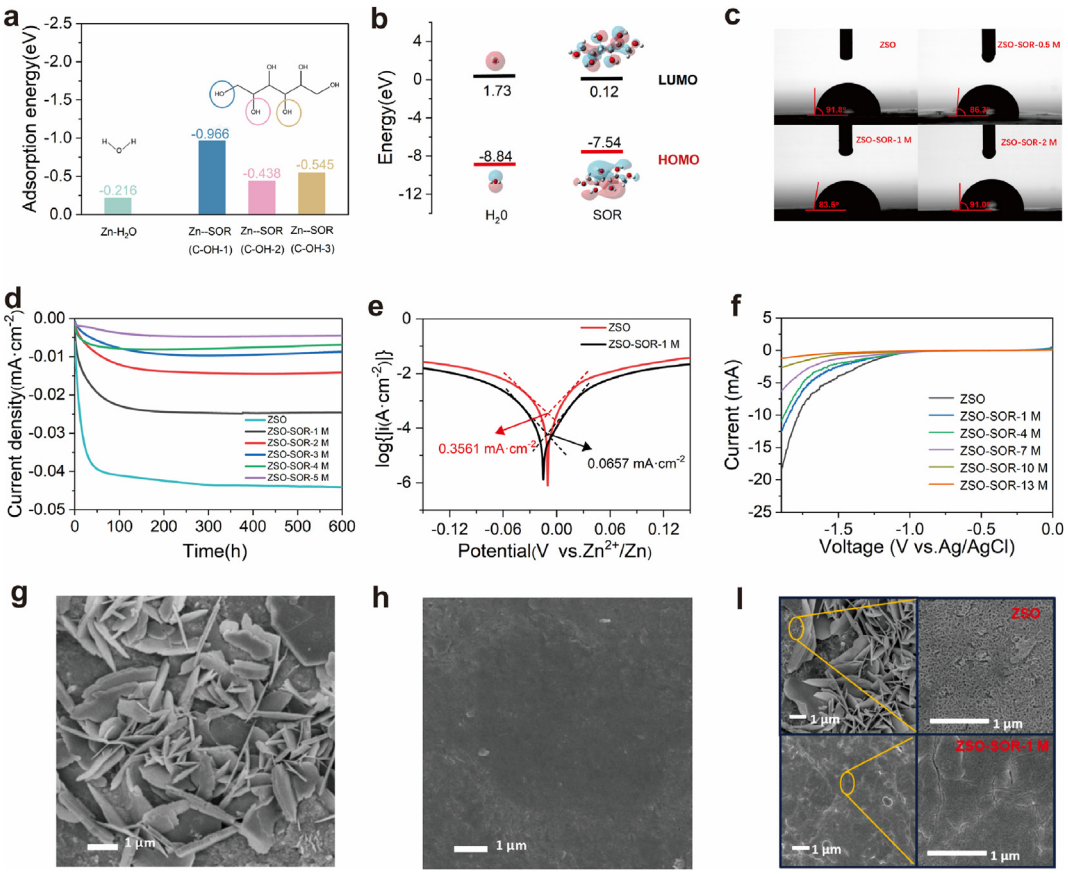

Fig. 3. (a) Adsorption energies with various adsorbates on the plane of Zn. (b) LUMO and HOMO iso-surface of H_2O and SOR molecules. (c) Contact angle between ZSO-SOR-x M and Zn interface. (d) Chronoamperograms of the Zn electrodes in Zn/Zn symmetric cell at an overpotential of −150 mV. (e) The Tafel plots of Zn/Zn cell with ZSO and ZSO-SOR-1 M. (f) Linear sweep voltammetric curves of ZSO-SOR-x M. Scanning electron microscopic observations of Zn electrodeposition process with (g) ZSO and (h) ZSO-SOR-1 M electrolyte after 5 cycles of plating, and (i) ZSO and ZSO-SOR-1 M electrolyte after 100 cycles of plating.

electrolyte continued to increase, indicating that there is a long-term 2D Zn^{2+} ion diffusion mode during this period (Fig. 3d). For the ZSO-SOR-1 M electrolyte, with a stable plateau after a short current elevation, transverse ion diffusion was significantly inhibited, which is reflected in the slow current growth rate and in turn inhibits the growth of Zn dendrites, furthermore, other concentrations of the modified electrolytes also had varying degrees of plateau conditions. The Tafel plots of Zn/Zn symmetric cells with the ZSO-SOR-1 M electrolyte had a lower exchange current density (0.0657 $mA \cdot cm^{-2}$) than those with the ZSO electrolyte (0.3561 $mA \cdot cm^{-2}$), implying a considerably enhanced suppression of corrosion kinetics (Fig. 3e) [29]. Apart from Zn corrosion, hydrogen evolution is also parasitic in the Zn plating/stripping process, which was estimated by linear sweep voltammetry (LSV) (Fig. 3f), with the increase of the concentration, the voltage range of the current response became wider, which confirms that the addition of sorbitol can effectively reduce the hydrogen evolution of water-based electrolyte by reducing the activity of water molecules, and the side reaction can be effectively inhibited.

Scanning electron microscope was employed to visualize the Zn electrodeposition process. The tip of the Zn electrode without additives was not uniform after five cycles of plating (Fig. 3g), and vertical Zn dendrites and the morphology of basic Zn sulfate, a loose side reaction product, could be seen. In contrast, the electrode in the ZSO-SOR-1 M electrolyte showed a flat surface and compact electrodeposition (Fig. 3h), which indicates that the addition of SOR greatly inhibited the side reaction and the generation of dendrites. The Zn electrode after 100 cycles was disassembled from the symmetrical cells (Fig. 3i). In the ZSO electrolytes, upright dendritic Zn dendrites were more rampant than 5-cycle dendritic cells, with the potential to short-circuit by penetrating the diaphragm. At the same time, combined with the results of XRD, the surface morphological analysis shows the serious side reactions on the surface. Through the expanded observation some non-dendritic areas, it is found that the loose alkaline Zn sulfate morphology filled the Zn anode with cracks and pores, while Zn hydroxide sulfate, which adhered closely to the surface of Zn crystals, may be detrimental to electron diffusion and the direction of Zn deposition. Whereas the smooth surface morphology was found for the ZSO-SOR-1 M counterpart, supporting the above mentioned, that is, the addition of SOR changes the solvation structure, restructures the interfacial chemistry, the decomposition of water molecules at the interface is inhibited, resulting in a less alkaline environment. The side reactions under the joint action were better inhibited, which is consistent with the corrosion current calculated by the previously measured Tafel curve.

Compared with inorganic materials such as MnO_2 (Figure S7), due to the restriction of water molecular activity and concentration polarization, the H^+/Zn^{2+} coinsertion process was hindered [30]. Organic materials have the advantages of low cost, light weight, diverse structure and high synthesis controllability, in addition to the redox active center of organic materials is usually exposed to the surface of the molecule and can be directly combined with the carrier [31], and its embedding mechanism is more compatible with our proposed electrolyte ZSO-SOR-1 M. Therefore, the full cell with PNDA as the cathode and fresh Zn foil as the anode were assembled to evaluate the applicability of this additive strategy. PNDA is a new organic cathode material reported recently, which has high theoretical specific capacity and good magnification performance. As confirmed by the FTIR (Figure S8), the characteristic peaks belonging to C=C, C=N and C−N stretching vibrations were observed near 1597, 1530 and 1298 cm^{-1}, respectively, which are consistent with literature reports, suggesting that the PNDA was successfully synthesized [32]. The CV curve of Zn/PNDA full cell shows redox peaks in the ZSO-SOR-1 M electrolyte in Fig. 4a, corresponding to the redox process of −NH− in the charge/discharge stage, but the specific Zn^{2+} storage mechanism needs to be further studied.

We have tested the performance of Zn/PNDA full cell. As shown in Fig. 4b, compared with the ZSO electrolyte, Zn/PNDA full cell with the ZSO-SOR-1 M electrolyte shows excellent performance. The positive electrode material had undergone a short activation process at the early stage of the cycle, after the activation was completed, the specific discharge capacity of the whole battery was stable at about 93 $mAh \cdot g^{-1}$ at a current density of 1 $A \cdot g^{-1}$ (about 2.9C), and the specific discharge capacity still reached 92.6 $mAh \cdot g^{-1}$ after 2300 cycles. At the same time, the CE of the whole battery stabilized at about 99.5% after activation, indicating that the Zn anode had good cyclic reversibility in the ZSO-SOR-1 M modified electrolyte. When the current densities ranged 1C, 2C, 4C, 6C, 8C, 10C and 20C (Fig. 4d), the discharge capacities of the battery became 100 $mAh \cdot g^{-1}$, 91 $mAh \cdot g^{-1}$, 84 $mAh \cdot g^{-1}$, 81 $mAh \cdot g^{-1}$, 80 $mAh \cdot g^{-1}$, 80 $mAh \cdot g^{-1}$, 79 $mAh \cdot g^{-1}$, respectively. When the current density was 30C, the discharge capacity could still reach 78.9 $mAh \cdot g^{-1}$, and the discharge capacity of

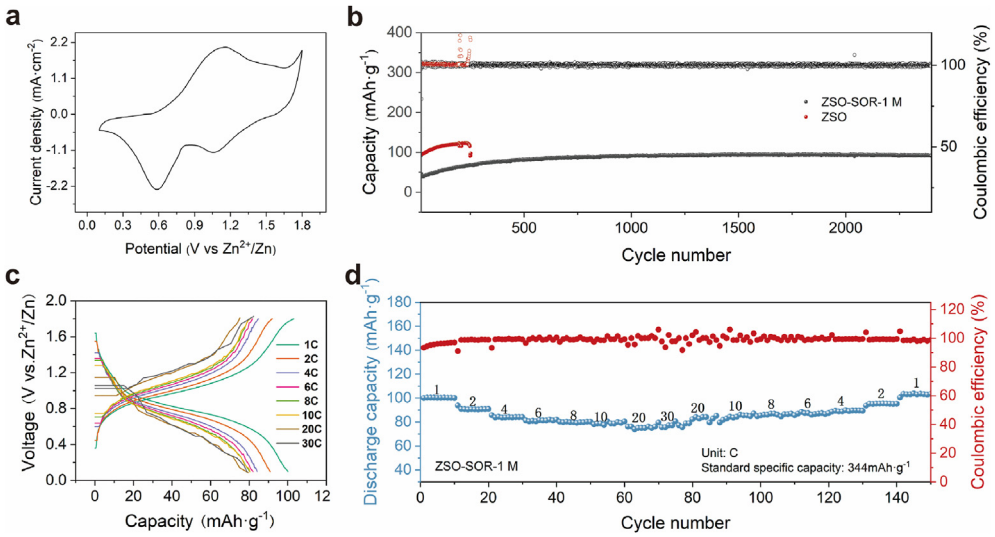

Fig. 4. Electrochemical performance of the Zn/PNDA full cells. (a) CV curve of the full cell. (b) Long-term cycling performance plots of the Zn/PNDA cells at a current density of 1 A·g^{-1} on the ZSO-SOR-1 M electrolyte. (c) Typical charge/discharge profiles of ZSO-SOR-1 M electrolyte at various rates from 1 C to 30 C. (d) Rate performance curves of ZSO-SOR-1 M electrolyte with various current densities ranging from 1 C to 30 C.

the battery did not fluctuate greatly with the current density. In short, the excellent electrochemical performance of the Zn/PNDA full cell indicates that the modified electrolyte has good compatibility with the organic cathode material and the excellent rate performance of the full cell, while ensuring the high reversibility of the Zn anode.

5. Conclusions

In summary, the hydroxy-rich sorbitol was chosen as the additive in commonly used $ZnSO_4$ electrolyte to realize superior Zn plating/stripping stability. The improvement mechanism of sorbitol additive was determined by combining various strategies including morphological characteristics, theoretical simulation and calculations, and electrochemical analytical characterization. On the one hand, the strong interaction between sorbitol and Zn^{2+} made it enter the solvation shell, reducing the proportion of bound water, and formed an intermolecular hydrogen bond network between sorbitol and water molecules, lowering the activity of free water molecules, thus limiting various side reactions to a certain extent, as also proved by the corrosion and HER properties. On the other hand, the good contact and adsorption between sorbitol and the Zn anode interface also hindered the direct contact between water molecules and the Zn anode, which reduce the decomposition of water molecules on the interface, inhibit the formations of various side reaction products and dendrites, and further help to improve the stability of Zn anode. Using a ZSO-SOR-1 M modified electrolyte, the symmetric Zn/Zn cell achieved a long lifetime of 2000 h for the reversible plating/stripping at 1 mAh·cm^{-2}, and the CE of the asymmetric Zn/Cu cell was as high as 99.6%. The constructed Zn/PNDA cell can be stably discharged for 2300 times at 1A·g^{-1} with a good capacity retention rate. Further studies showed that the introduction of sorbitol additive agent could effectively prevent the growths of Zn dendrite and inert by-products, as well as the hydrogen evolution. This work provides a common cost-effective additive strategy for achieving high performance aqueous zinc ion batteries with a long-life span.

Conflict of interest

The authors decline no competing interest.

Acknowledgements

This study was supported by the National Natural Science Foundation of China (22279063, 52001170), Tianjin Natural Science Foundation (22JCYBJC00590), and the Fundamental Research Funds for the Central Universities. We thank the Haihe Laboratory of Sustainable Chemical Transformations for financial support.

Supporting Information

Supporting Information for this article is available at the website of J. Electrochem.

References

[1] Armand M, Tarascon J M. Building better batteries[J]. Nature, 2008, 451(7179): 652−657.

[2] Liang J, Li X, Zhao Y, Goncharova L V, Wang G, Adair K R, Wang C, Li R, Zhu Y, Qian Y, Zhang L, Yang R, Lu S, Sun X. *In situ* Li_3PS_4 solid-state electrolyte protection layers for

superior long-life and high-rate lithium-metal anodes[J]. Adv. Mater., 2018, 30(45): 1804684.

[3] Chang N N, Li T Y, Li R, Wang S N, Yin Y B, Zhang H M, Li X F. An aqueous hybrid electrolyte for low-temperature zinc-based energy storage devices[J]. Energy Environ. Sci., 2020, 13(10): 3527−3535.

[4] Wang Y G, Yi J, Xia Y Y. Recent progress in aqueous lithium-ion batteries[J]. Adv. Energy Mater., 2012, 2(7): 830−840.

[5] Jia X X, Liu C F, Neale Z G, Yang J H, Cao G Z. Active materials for aqueous zinc ion batteries: synthesis, crystal structure, morphology, and electrochemistry[J]. Chem. Rev., 2020, 120(15): 7795−7866.

[6] Cai Z, Wang J, Sun Y. Anode corrosion in aqueous Zn metal batteries[J]. eScience, 2023, 3(1): 100093.

[7] Wang F, Borodin O, Gao T, Fan X, Sun W, Han F, Faraone A, Dura J A, Xu K, Wang C. Highly reversible zinc metal anode for aqueous batteries[J]. Nat. Mater., 2018, 17(6): 543−549.

[8] Suo L M, Borodin O, Gao T, Olguin M, Ho J, Fan X L, Luo C, Wang C S, Xu K. "Water-in-salt" electrolyte enables high-voltage aqueous lithium-ion chemistries[J]. Science, 2015, 350(6263): 938−943.

[9] Sun P, Ma L, Zhou W H, Qiu M J, Wang Z L, Chao D L, Mai W J. Simultaneous regulation on solvation shell and electrode interface for dendrite-free Zn ion batteries achieved by a low-cost glucose additive[J]. Angew. Chem. Int. Ed., 2021, 60(33): 18247−18255.

[10] Cao J, Zhang D D, Zhang X Y, Zeng Z Y, Qin J Q, Huang Y H. Strategies of regulating Zn^{2+} solvation structures for dendrite-free and side reaction-suppressed zinc-ion batteries[J]. Energy Environ. Sci., 2022, 15(2): 499−528.

[11] Ma G Q, Miao L C, Dong Y, Yuan W T, Nie X Y, Di S L, Wang Y Y, Wang L B, Zhang N. Reshaping the electrolyte structure and interface chemistry for stable aqueous zinc batteries[J]. Energy Storage Mater., 2022, 47: 203−210.

[12] Ye Z, Cao Z, Chee M OL, Dong P, Ajayan P M, Shen J, Ye M. Advances in Zn-ion batteries via regulating liquid electrolyte[J]. Energy Storage Mater., 2020, 32: 290−305.

[13] Cao L S, Li D, Hu E Y, Xu J J, Deng T, Ma L, Wang Y, Yang X Q, Wang C S. Solvation structure design for aqueous Zn metal batteries[J]. J. Am. Chem. Soc., 2020, 142(51): 21404−21409.

[14] Shi J Q, Sun T J, Bao J Q, Zheng S B, Du H H, Li L, Yuan X M, Ma T, Tao Z L. "Water-in-deep eutectic solvent" electrolytes for high-performance aqueous Zn-ion batteries [J]. Adv. Funct. Mater., 2021, 31(23): 2102035.

[15] Zhang Q, Ma Y L, Lu Y, Li L, Wan F, Zhang K, Chen J. Modulating electrolyte structure for ultralow temperature aqueous zinc batteries[J]. Nat. Commun., 2020, 11(1): 4463.

[16] Li T C, Lin C, Luo M, Wang P, Li D S, Li S, Zhou J, Yang H Y. Interfacial molecule engineering for reversible Zn electrochemistry[J]. ACS Energy Lett., 2023, 8(8): 3258−3268.

[17] Li D, Cao L S, Deng T, Liu S F, Wang C S. Design of a solid electrolyte interphase for aqueous Zn batteries[J]. Angew. Chem. Int. Ed., 2021, 60(23): 13035−13041.

[18] Qiu M J, Ma L, Sun P, Wang Z L, Cui G F, Mai W J. Manipulating interfacial stability via absorption-competition mechanism for long-lifespan Zn anode[J]. Nano-Micro Lett., 2022, 14: 31.

[19] Yu L, Huang J, Wang S J, Qi L H, Wang S S, Chen C J. Ionic liquid "water pocket" for stable and environment-adaptable aqueous zinc metal batteries[J]. Adv. Mater., 2023, 35(21): 2210789.

[20] Malde A K, Zuo L, Breeze M, Stroet M, Poger D, Nair P C, Oostenbrink C, Mark A E. An automated force field topology builder (atb) and repository: version 1.0[J]. J. Chem. Theory Comput., 2011, 7(12): 4026−4037.

[21] Hess B. GROMACS 4: Algorithms for highly efficient, load-balanced, and scalable molecular simulation[J]. Abstr. Papers Am. Chem. Soc., 2009, 237: 435−447.

[22] Lomas J S, Joubert L, Maurel F. Association of symmetrical alkane diols with pyridine: DFT/GIAO calculation of ^{1}H NMR chemical shifts[J]. Magn. Reson. Chem., 2016, 54(10): 805−814.

[23] Sun T J, Nian Q S, Ren X D, Tao Z L. Hydrogen-bond chemistry in rechargeable batteries[J]. Joule, 2023, 7(12): 2700−2731.

[24] Wei J, Zhang P B, Shen T Y, Liu Y Z, Dai T F, Tie Z X, Jin Z. Supramolecule-based excluded-volume electrolytes and conjugated sulfonamide cathodes for high-voltage and long-cycling aqueous zinc-ion batteries[J]. ACS Energy Lett., 2023, 8(1): 762−771.

[25] Lu H T, Zhang X L, Luo M H, Cao K S, Lu Y H, Xu B B, Pan H G, Tao K, Jiang Y Z. Amino acid-induced interface charge engineering enables highly reversible Zn anode[J]. Adv. Funct. Mater., 2021, 31(45): 2103514.

[26] Liu M Y, Yuan W T, Ma G Q, Qiu K Y, Nie X Y, Liu Y C, Shen S G, Zhang N. *In-situ* integration of a hydrophobic and fast-Zn^{2+}-conductive inorganic interphase to stabilize Zn metal anodes[J]. Angew. Chem. Int. Ed., 2023, 62(27): e202304444.

[27] Chen W Y, Guo S, Qin L P, Li L Y, Cao X X, Zhou J, Luo Z G, Fang G Z, Liang S Q. Hydrogen bond-functionalized massive solvation modules stabilizing bilateral interfaces[J]. Adv. Funct. Mater., 2022, 32(20): 2112609.

[28] Zhao Z M, Zhao J W, Hu Z L, Li J D, Li J J, Zhang Y J, Wang C, Cui G L. Long-life and deeply rechargeable aqueous Zn anodes enabled by a multifunctional brightener-inspired interphase[J]. Energy Environ. Sci., 2019, 12(6): 1938−1949.

[29] Miao L C, Wang R H, Di S L, Qian Z F, Zhang L, Xin W L, Liu M Y, Zhu Z Q, Chu S Q, Du Y, Zhang N. Aqueous electrolytes with hydrophobic organic cosolvents for stabilizing zinc metal anodes[J]. ACS Nano., 2022, 16(6): 9667−9678.

[30] Li C C, Hu L, Ren X Y, Lin L, Zhan C Z, Weng Q S, Sun X Q, Yu X L. Asymmetric charge distribution of active centers in small molecule quinone cathode boosts high-energy and high-rate aqueous zinc-organic batteries[J]. Adv. Funct. Mater., 2024, 34(16): 2313241.

[31] Gao X, Wu H W, Li W J, Tian Y, Zhang Y, Wu H, Yang L, Zou G Q, Hou H S, Ji X B. H^{+}-insertion boosted α-MnO_2 for an aqueous Zn-ion battery[J]. Small, 2020, 16(5): 1905842.

[32] Zhao Y, Wang Y N, Zhao Z M, Zhao J W, Xin T, Wang N, Liu J Z. Achieving high capacity and long life of aqueous rechargeable zinc battery by using nanoporous-carbon-supported poly(1,5-naphthalenediamine) nanorods as cathode[J]. Energy Storage Mater., 2020, 28: 64−72.

基于山梨醇添加剂电解质的可逆锌电化学

孙琼[a]，杜海会[a]，孙田将[a]，李典涛[a]，程敏[a]，梁静[a,*]，李海霞[a,b,*]，陶占良[a]

[a] 南开大学先进能源材料化学教育部重点实验室，天津 300071

[b] 中国石油和化工行业太阳能电池电极材料重点实验室，苏州科技大学化学与生命科学学院，江苏 苏州 215009

摘要

在水系锌离子电池中，锌枝晶、析氢，以及不稳定的锌界面使其表现出低的库仑效率和较差的循环性能。本文选用富含羟基的山梨醇作为电解质添加剂，用于重塑锌的溶剂化结构和调整锌阳极界面化学，有效抑制了水的分解以及锌枝晶的产生。一方面山梨醇与水分子强相互作用可以形成氢键网络，改变 Zn^{2+}离子与水分子之间的溶剂化壳层，减少结合水的比例，降低游离水活性；另一方面山梨醇和 Zn 阳极界面之间的吸附调节了 Zn 阳极表面结构，减少其与水分子的接触，获得热力学稳定、高度可逆的 Zn 电化学沉积/溶解。结果表明，含有山梨醇添加剂的 Zn/Zn 对称电池在 1 $mA·cm^{-2}$ 和 1 $mAh·cm^{-2}$ 的条件下实现了长达 2000 小时的循环寿命，在 5 $mA·cm^{-2}$ 和 5 $mAh·cm^{-2}$ 条件下也能超过 250 小时的循环寿命。添加山梨醇的 Zn/Cu 不对称电池获得了 99.6%的库仑效率，比纯 2 $mol·L^{-1}$ $ZnSO_4$ 电解质具有更高性能。Zn/PNDA 全电池可在 1 $A·g^{-1}$ 电流密度下稳定放电超过 2300 次，并且保持了较好的电池容量。本论文通过向传统电解质中添加安全无毒的山梨醇，提升了对锌阳极界面的保护作用以及循环性能，改善了锌的可逆沉积/溶解电化学性能，为高性能水系锌离子电池的探索提供了新思路。

关键词：水系锌离子电池；枝晶；山梨醇添加剂；溶剂化调节；界面调节